Electrostatic Layer-by-Layer Assembly of Poly(amido amine) Dendrimer/Conducting Sulfonated Polyaniline: Structure and Properties of Multilayer Films

Chun Li,[†] Koji Mitamura,[‡] and Toyoko Imae*,[†,‡]

Research Center for Materials Science and Graduate School of Science, Nagoya University, Chikusa, Nagoya 464-8602, Japan

ABSTRACT: The multilayers of poly(amido amine) dendrimer (fourth generation amine-terminated, $G4NH_2$) and conducting sulfonated polyaniline (SPANI) were successfully deposited onto solid substrates by alternatively dipping in SPANI and $G4NH_2$ solutions. Multilayer growth was monitored by ultraviolet−visible absorption spectroscopy and Fourier transform infrared-reflection absorption spectroscopy, which revealed an adsorption−desorption phenomenon, although it was sensitive to the concentration and pH of solutions. The average thickness of the SPANI/$G4NH_2$ bilayer obtained from X-ray reflectivity is much smaller than the diameter of $G4NH_2$ with an ideal spherical structure, suggesting that the dendrimer molecules in multilayers are highly compressed along the surface normal. Electron density profiles indicate that the multilayers are highly interpenetrated, and the thickness and molecular arrangement in the multilayers depend on the pH of $G4NH_2$ solutions. Cyclic voltammograms of the multilayers in acidic and neutral electrolyte solutions show that the multilayers have good physical and electrochemical stability. The photoelectric conversion response shows cathodic or anodic photocurrent depending on the bias voltage (i.e., on the oxidation state of SPANI). At higher potentials, it shows characteristics of an n-type semiconductor, whereas it behaves like a p-type semiconductor at lower potentials.

1. Introduction

Dendrimers are a class of synthetic polymers with an unusual three-dimensional highly branched structure composed of a core, repeating units, and end groups.[1,2] During the past two decades, much work has been concentrated on this area due to their crucial roles in making functional materials.[3−7] Poly(amido amine) dendrimers are a widely investigated group of dendritic polymers because they have a well-defined composition and constitution as well as a narrow molecular distribution and are commercial available.[1−3] Recently, the architecture of dendrimer-based monolayer and multilayer films has become a topic of increasing interest due to their various potential applications.[8−18]

The fabrication and characterization of conducting polymer films have been paid much attention in view of their multiple potential technological applications[19−24] such as light-emitting diode[19] and biosensor.[20,21] The traditional approaches to make films of this kind of materials included electropolymerization,[21,25,26] spin-casting of soluble derivatives,[27,28] and the Langmuir−Blodgett technique.[29,30] Electrostatic layer-by-layer assembly pioneered by Decher[31] has been exploited as an alternative method to get thin films. This method provides a simple means of coating a larger or irregular surface area in a controlled, defined manner[31,32] and has been found effective in processing conducting polymer films.[33−43] However, to date, there are a few reports concerning the electrically conductive dendrimer films.[44,45]

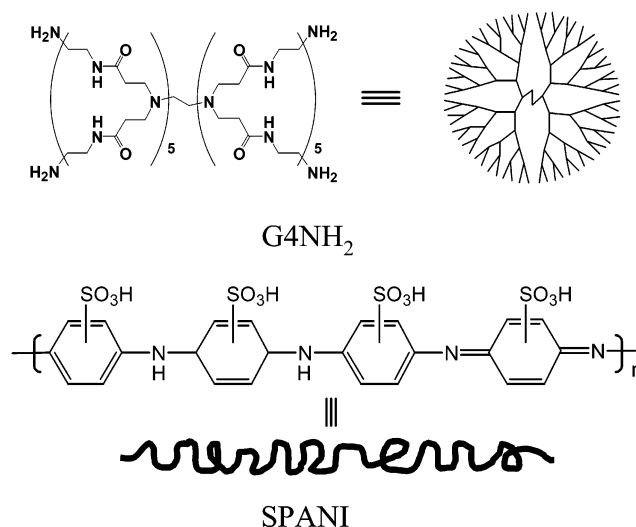In the present work, we report the deposition of electroactive multilayers consisting of sulfonated poly-

Figure 1. Schematic drawing of the chemical structures of $G4NH_2$ and SPANI.

aniline[46−50] (SPANI, as the polyanion) and fourth generation amine-terminated poly(amido amine) ($G4NH_2$, as the polycation) by the electrostatic layer-by-layer assembly. The process of the growth was followed by ultraviolet−visible (UV−vis) absorption spectroscopy and Fourier transform infrared-reflection absorption (FTIR-RA) spectroscopy. The organized structure and surface morphology of the multilayers were investigated by X-ray reflectometry and atomic force microscopy (AFM). The effects of concentration and pH of the solutions on the film growth and the structure of the resulting multilayers were discussed. The redox and photoelectric conversion properties of the SPANI/$G4NH_2$ multilayers were investigated by cyclic voltammetry (CV).

* Correspondence author: Fax + 81-52-789-5912; Tel + 81-52-789-5911; e-mail imae@nano.chem.nagoya-u.ac.jp.
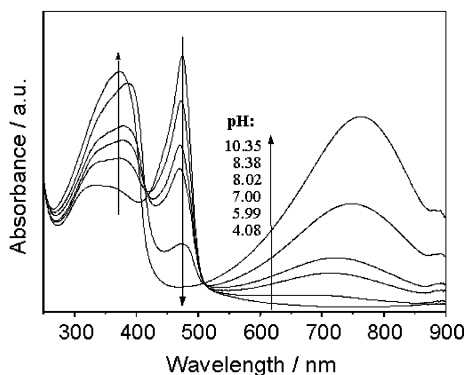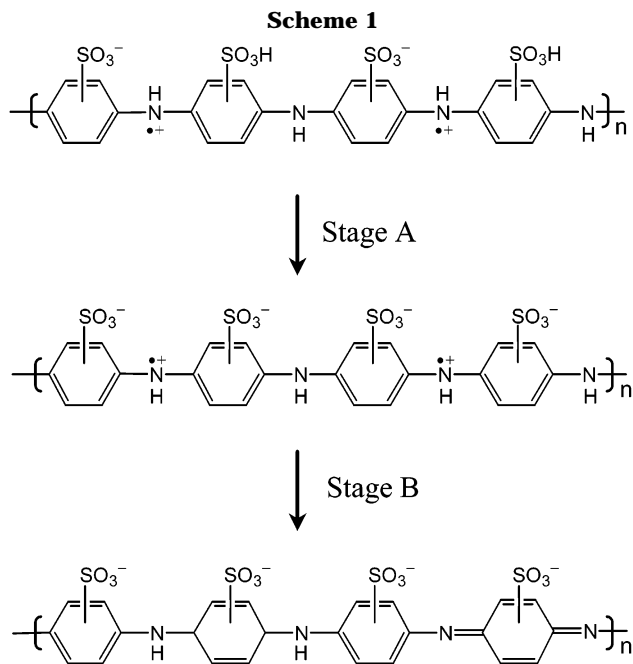† Research Center for Materials Science.
‡ Graduate School of Science.

Figure 2. UV–vis absorption spectra of 1 mM SPANI solutions at different pH values.

Scheme 1

Figure 3. UV–vis absorption spectra of the deposition process of SPANI/G4NH$_2$ multilayers (for a 1 mM SPANI concentration) on glass slide with inset showing the absorbance at 475 nm against the layer number n for various SPANI concentrations: closed square, 0.1 mM; closed circle, 1 mM; closed triangle, 5 mM.

Figure 4. Influence of ion strength on the growth of SPANI/G4NH$_2$ multilayers: closed square, $C_{NaCl} = 0$; closed circle, $C_{NaCl} = 0.2$ M; closed triangle, $C_{NaCl} = 0.4$ M.

2. Experimental Section

2.1. Materials. Fourth generation amine-terminated poly-(amido amine) dendrimer (G4NH$_2$, 10 wt % methanol solution, $M_w = 14\ 215$), poly(anilinesulfonic acid) (SPANI, aqueous 5 wt % solution, degree of sulfonation ~100%, $M_n = 10\ 000$), 3-aminopropylethoxysilane (APS), and β-mercaptoethylamine (MEA) hydrochloride were used as received from Aldrich Chemical Co. The chemical structures for G4NH$_2$ and SPANI are illustrated in Figure 1. Toluene (anhydrous), methanol, ethanol, and sodium chloride were analytical grade and purchased from Wako Pure Chemical Industries, Ltd. The aqueous solutions were prepared with ultrapure water (18.3 MΩ), which was prepared using a Milli-Q filtration unit from the Millipore Corp.

2.2. Substrates. Glass slides, Au substrates (200 nm thick Au film evaporated on glass with a 150 nm chromium adhesion layer), and silicon wafers were immersed in a fresh piranha solution (v/v = 1:3, 30% H$_2$O$_2$/98% H$_2$SO$_4$) (*caution: piranha solution is very corrosive and must be treated with extreme care; it reacts violently with organic materials*) at 80 °C for ca. 20 min, followed by thorough rinsing with copious Millipore water. ITO-coated glass slides were cleaned by sonication for 5 min in aqueous alkali detergent, rinsing with ample water, and then these slides were dipped in piranha solution for 10 s to enhance the hydrophilic nature of the surface to ensure the proper anchoring of the siloxane groups without destroying the conductive oxide layer. The glass, silicon, and ITO-coated glass substrates were silanized with APS in anhydrous toluene solution (5% volume) for 1 h at room temperature. After several
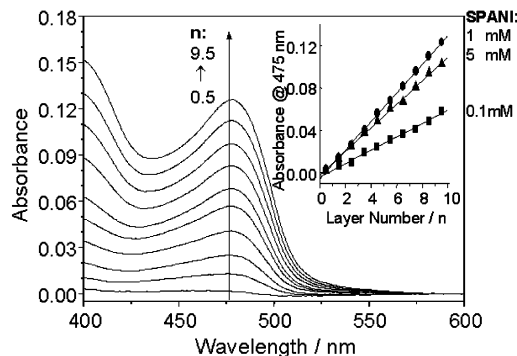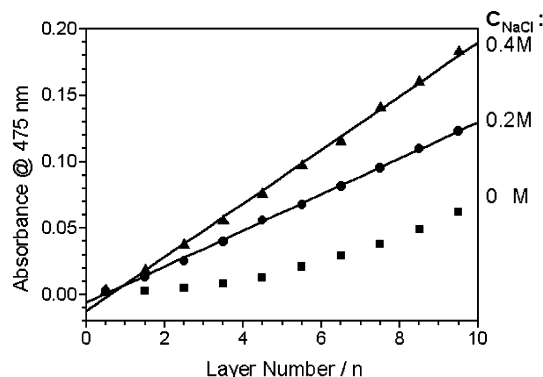
cycles sonication and rinsing with fresh toluene and methanol, the substrates were heated to 105 °C for 1 h to allow the condensation reaction of the siloxane to proceed. The APS layer was positively charged by immersion in dilute HCl solution, and the substrates were stored in pure water prior to use. The surface of Au substrates was charged by immersion of the slides for 1 h in an ethanol solution of MEA hydrochloride (1 mM), followed by rinsing, and then a uniform positively charged surface was created.

2.3. Film Deposition. Aqueous G4NH$_2$ solution with a concentration of 1 mg cm^3 and a 1 mM SPANI solution (with respect to monomer unit, aminobenzenesulfonic acid) were prepared for multilayer deposition. The ionic strength of the polyelectrolytes (both G4NH$_2$ and SPANI) was adjusted with sodium chloride to 0.2 M, and their pH values were adjusted to 6.0 with dilute HCl or NaOH. These typical polyelectrolyte solutions described above were used to deposit the multilayers unless otherwise specified. During the study of ion strength effects on the multilayer growth, the ion strength of SPANI and G4NH$_2$ solutions was kept at the same level. Multilayers were deposited by alternately dipping positively charged substrates into aqueous solutions of SPANI and G4NH$_2$. The substrates were dipped in each solution for 10 min and subsequently rinsed three times by dipping in water (1 min each). After each deposition and rinsing step, the samples were dried with a gentle flow of compressed air.

2.4. Measurements. UV–vis absorption spectra were recorded on a Shimadzu UV-2200 spectrometer, and a 1 mm-path length quartz cuvette was used for the measurement of solution spectra. FTIR-RA spectra were recorded on a Bio-Rad FTS 575C FT-IR spectrometer using a Harrick reflectance attachment with an incidence angle of 75°. AFM observations were performed in the tapping mode on an AFM Nanoscope III (Digital Instruments, Inc.). A crystalline silicon tip on a
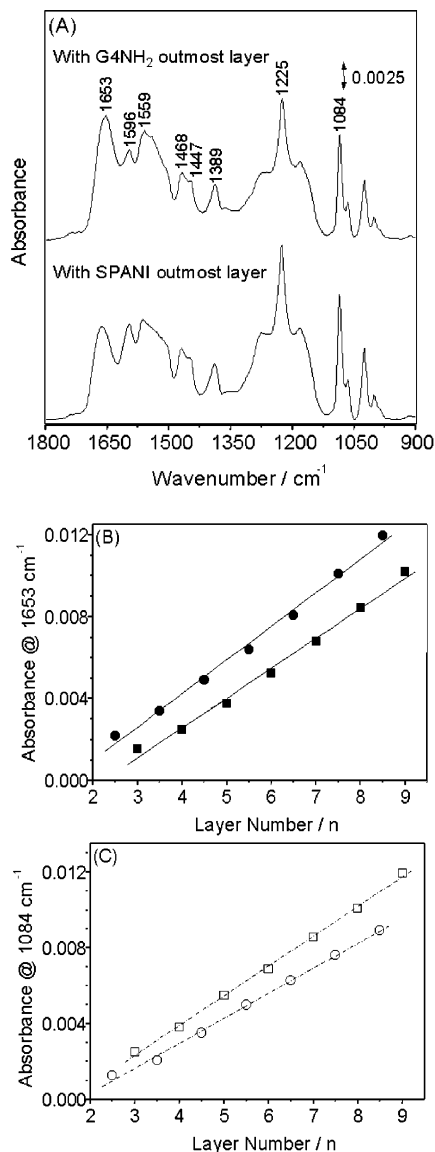
Figure 5. (A) FTIR-RA spectra of nine-bilayer SPANI/G4NH₂ multilayers prepared from pH 6.0 SPANI/pH 6.0 G4NH₂ solutions with SPANI (bottom) and G4NH₂ (top) as the outmost layer. (B) The peak intensities of the amide I ($\sim$1653 cm^{-1}) and (C) symmetric OSO stretching ($\sim$1084 cm^{-1}) modes against the layer number n.

Figure 6. (A) Peak intensities of the amide I ($\sim$1653 cm^{-1}) and (B) symmetric OSO stretching ($\sim$1084 cm^{-1}) modes against the layer number n. The multilayer was deposited from a pH 6.0 SPANI/pH 9.8 G4NH₂ solution.

cantilever was used. X-ray reflectivity measurements were performed on a RINT 2000 (Rigaku Co., Ltd.) diffractometer with Cu Kα irradiation (1.54 Å). X-ray data were collected with a step width of 0.02° (in 2θ). Voltammetric and potentiostatic experiments were performed in a one-compartment, three-electrode electrochemical cell with the use of a Hokuto-Denko model HZ-3000 automatic polarization system. The working electrode was SPANI/G4NH₂-covered Au or ITO substrates, and a Pt wire was used as counter electrode. All potentials were referred to a saturated calomel electrode (SCE). The photoelectric conversion measurements were carried out with polychromatic irradiation from EX250 UV light source (Hoya-Schott) on an electrochemical cell discussed above.

3. Results and Discussion

3.1. UV−vis Absorption Spectra of Aqueous SPANI Solutions and Electric Structure of SPANI. SPANI can be easily dissolved in water even in an acidic solution. The distinct improvement of its solubility in comparison with the parent polyaniline and partly
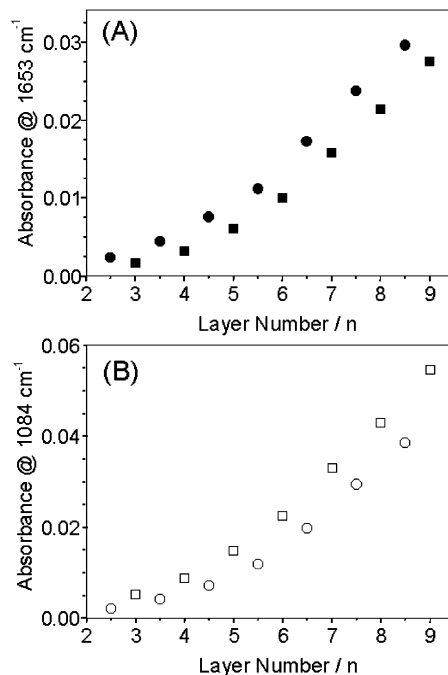
sulfonated polyaniline (50% sulfonation) reported previously[46−50] indicates that part of sulfonic groups exists in the form of $-SO_3H$ and can dissociate into a $-SO_3^-$ group and free proton. However, the sulfonated polyaniline with lower sulfonation degree is insoluble in an acidic solution because the protons in $-SO_3H$ are bound to an imino nitrogen in polyaniline main chains and an intramolecular salt is formed.[50] This result is further proved by the fact that the acidity (pH) of the SPANI solution is dependent on its concentration.

Figure 2 shows UV−vis absorption spectra for aqueous 1 mM SPANI solutions at different pH values. For a SPANI solution with a pH of 4.08 (no adjustment), a broad absorption peak due to $\pi-\pi^*$ transition[51] of the benzenoid ring around 334 nm and an absorption peak due to polaron band transition[47−50] at 474 nm are observed, indicating that SPANI is in the doped state.[47−50] To fully understand the electric structure of SPANI at various acidic doping levels and find optimum conditions for the SPANI/G4NH₂ multilayer deposition, UV−vis absorption spectra at various pH values were recorded. Before neutralization of the acidic state, the SPANI is in the self-doped state as reflected by the presence of polaron band transition at 474 nm (Scheme 1). With increasing pH value, the polaron band decreases gradually, and a strong absorption due to exciton transition of the quinoid rings[49,50] at 700−765 nm grows simultaneously. On the basis of the pH-dependent UV−vis absorption spectra, we believe that two stages were involved in the neutralization process as reported previously.[49,50] In the first stage (A), only free protons were neutralized (pH ≤ 6.0) since the spectra show no distinct difference in the range of pH 4.08−6.0; the second stage (B) involves the conversion of polaron structure to quinoid unit by the removal of the protons on imine nitrogen atoms. In this work, aqueous SPANI solution with pH 6.0 was chosen for the multilayer deposition, since at this point the SPANI are negatively charged and the strong polaron band transi-
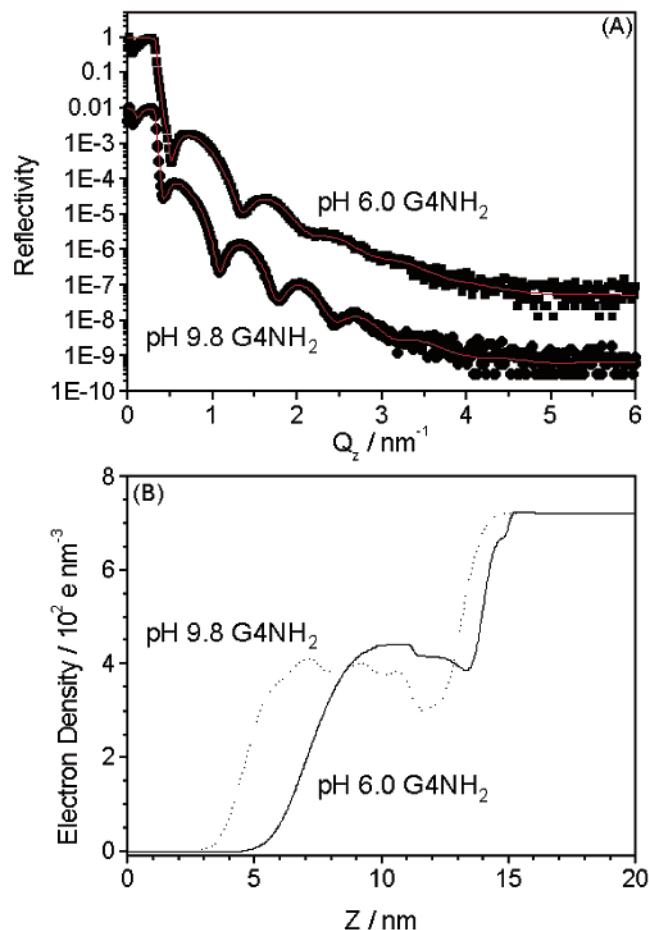
Figure 7. (A) X-ray reflectograms for four-bilayer multilayers on silicon substrates deposited from pH 6.0 SPANI/pH 6.0 G4NH$_2$ (square) and pH 6.0 SPANI/pH 9.8 G4NH$_2$ (circle) solutions. The red lines denote the best-fit calculated reflectivity to the experimental data. (B) Variation of the electron density as a function of thickness Z corresponding to the fit of the experimental reflectivity curves: solid line corresponds to the film prepared from a pH 6.0 SPANI/pH 6.0 G4NH$_2$ solution; dotted line refers to the film prepared from a pH 6.0 SPANI/pH 9.8 G4NH$_2$ solution.
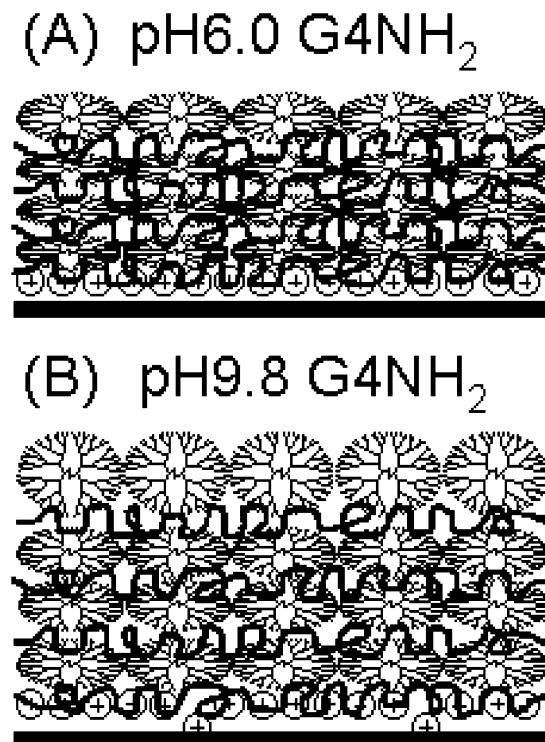

Figure 8. Schematic illustration of possible arrangements of SPANI and G4NH$_2$ in the multilayers: (A) the multilayer prepared from a pH 6.0 SPANI and pH 6.0 G4NH$_2$ solution; (B) the multilayer prepared from a pH 6.0 SPANI and pH 9.8 G4NH$_2$ solution. The charges on SPANI and G4NH$_2$ were omitted here.

tion around 474 nm can be used to follow the multilayer growth.

3.2. Optimization of SPANI/G4NH$_2$ Multilayer Deposition. Figure 3 shows UV–vis absorption spectra of SPANI/G4NH$_2$ multilayers on a glass substrate with 0.5–9.5 layers. An integer number of SPANI/G4NH$_2$ multilayers used here denotes that G4NH$_2$ is the outmost layer and multilayers contain the whole bilayers, whereas the multilayers with an additional 0.5 layer are terminated with SPANI. The absorption peak at 475 nm originated from SPANI polaron transition was used to monitor the multilayer deposition. It is clear from the inset of Figure 3 that the multilayers grew linearly with sequential deposition of the SPANI and G4NH$_2$ over the range of SPANI solution concentrations studied, suggesting successful film deposition by electrostatic layer-by-layer assembly. As indicated by the slopes of these lines, the amount of SPANI deposited per bilayer initially increases with increasing solution concentration and attains the maximum around 1 mM and then decreases, which is different from those of linear polyelectrolytes[33–36] and should be related to the adsorption–desorption equilibrium of SPANI and G4NH$_2$. When SPANI solutions of high concentrations are used

to deposit multilayers, SPANI molecules tend to extract more G4NH$_2$ dendrimers adsorbed in the previous step, which make the surface charge density decrease and less SPANI was adsorbed.

Figure 4 illustrates the role that the ion strength of polyelectrolyte solutions plays in the multilayer deposition. It is well-known that for relatively flexible linear polyelectrolyte chains the thickness and conformation of the adsorbed polymer depend primarily on the level of the effective intrasegmental repulsion of the ions distributed along the chain,[31,32] which can be manipulated by changing the ionic strength of the polymer solution.[35,36] However, we cannot simply ascribe the differences observed in the amount of SPANI adsorbed from solutions with different ion strength to changes in the population of chain segments present as trains, loops, and tails due to its quite rigid structure within the main chains. Considering the thickness determined by X-ray reflectivity as discuss in section 3.4, we believe that the SPANI chains are adsorbing with highly extended conformations with low segmental density of loops and tails in the ion strength studied here. The enhancement of the adsorption of SPANI onto surfaces by adding salt to the solutions can be attributed to partially neutralize the net charge of the chains (shielding effect). On the other hand, at higher ion strength, the dendrimers take a more dense core dendritic structure,[52] and the surface charge density is lower than that at lower ion strength with more extended conformation. Therefore, more dendrimer molecules will be adsorbed on the film surface to balance the charges.

3.3. FTIR-RA Spectra of SPANI/G4NH$_2$ Films and the Adsorption–Desorption Process. As discussed in the above section, the amount of SPANI
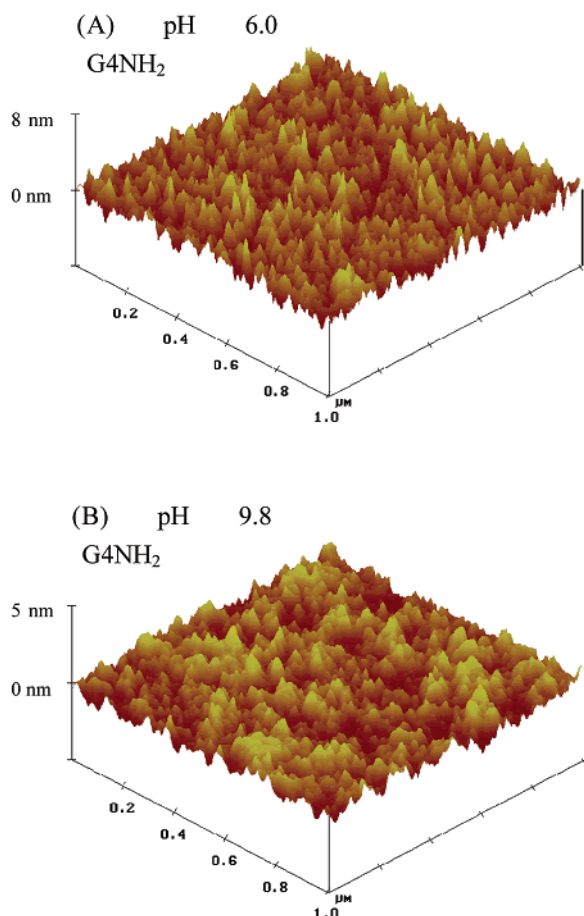
Figure 9. AFM images of four-bilayer SPANI/G4NH$_2$ films on silicon substrates. The notations of (A) and (B) are the same as Figure 8.
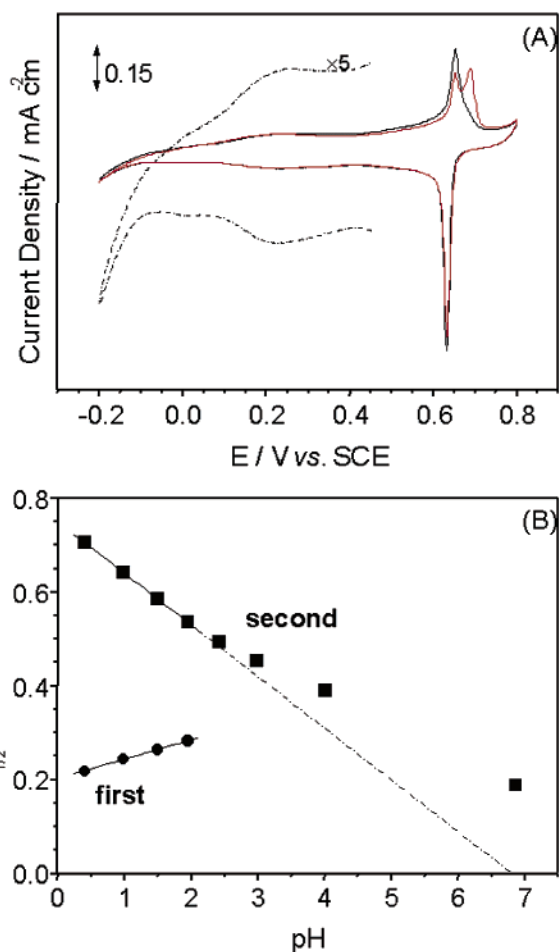

Figure 10. (A) CVs (50 mV s^{-1}) of nine-bilayer SPANI/G4NH$_2$ film in 0.1 M HCl: red line, first scan; black line, second scan. (B) Plots of $E_{1/2}$ (50 mV s^{-1}) against pH value of aqueous HCl solutions (for pH 4.01 and 6.86, buffer was used): circle, the first redox process; square, the second redox process. Linear lines were fitted at lower pH.

adsorption can be followed by UV–vis absorption spectra. To further investigate the adsorption and desorption of SPANI and G4NH$_2$ onto the surfaces, FTIR-RA spectroscopy was used to follow these processes.

G4NH$_2$ is a weak polyelectrolyte and can be protonated at terminals and branch points in aqueous solution, with the extent of protonation depending on the solution pH.[1,2,53] It has been shown that the primary amines at the dendritic terminals have higher pK_a than the tertiary ones at the branch points.[1] Therefore, the protonation strongly affects the conformation of dendrimers: at lower pH, greater molecular charge results in a more open structure with an expanded conformation due to the protonation of the tertiary amines and the charge–charge repulsions, whereas at higher pH, charges are only on the terminals and the dendrimer has a more condensed (dense core) structure.[53,54] To investigate the influences of this effect on the structure of the multilayers, pH 6.0 (full charged) and 9.8 (partly charged on the terminals) were chosen to deposit the multilayers, and FTIR-RA spectra were recorded after each adsorption step.

Figure 5A shows the FTIR-RA spectra for the nine-bilayer SPANI/G4NH$_2$ multilayers fabricated from the SPANI (pH 6.0) and G4NH$_2$ (pH 6.0) solutions with the SPANI (bottom) and G4NH$_2$ (top) as the outmost layer, respectively. The strong vibrations around 1653 and 1559 cm^{-1} are due to the internal amide groups of the G4NH$_2$.[55] The bands at 1468, 1447, and 1389 cm^{-1} are attributed to the CH$_2$ scissoring and wagging modes of the dendrimer.[55] The band at 1596 cm^{-1} is assigned to

the C=C ring stretching of the radical cation of imono-1,4-pheneylene in the SPANI main chain.[56] Strong asymmetric and symmetric OSO stretching bands from the sulfonic acid group appear at 1225 and 1084 cm^{-1}, respectively.[50] The peak intensities of the symmetric OSO stretching mode (1084 cm^{-1}) in SPANI and the amide I mode (1653 cm^{-1}) in G4NH$_2$ were plotted against the layer number to illustrate the adsorption–desorption behavior (Figure 5B). It can be seen that the amount of SPANI and G4NH$_2$ adsorption increases with increasing bilayer number (i.e., SPANI or G4NH$_2$ as outmost layer). Upon subsequent deposition of the dendrimer, the sulfonic peak decreases in intensity, suggesting that part of the adsorbed SPANI was desorbed during dendrimer adsorption due to the formation of SPANI/G4NH$_2$ complex, and similar changes were detected for dendrimer after the additional SPANI layer was deposited. These obvious desorption phenomena for SPANI and G4NH$_2$ at each subsequent deposition step are different from the electrostatic layer-by-layer assembly with both linear polyelectrolytes, in which no dramatic desorption was detected.[31,32] Similar adsorption–desorption behavior has been reported for electrostatic layer-by-layer deposited films using one low molecular weight component.[57] Although there exists a complicated adsorption–desorption phenomenon, the deposition process is still reproducible from layer to
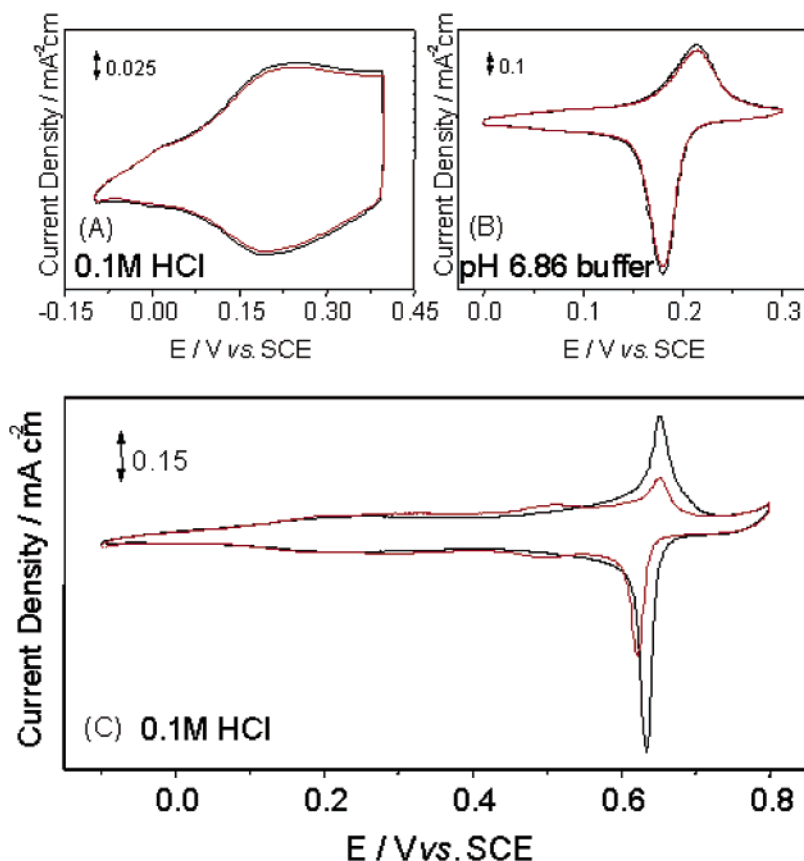
Figure 11. CVs of nine-bilayer SPANI/G4NH₂ multilayers. (A) Second scan (black) and 500th scan (red) from −0.1 to 0.4 V in a 0.1 M HCl solution; (B) second scan (black) and 500th scan (red) from 0 to 0.3 V in a neutral electrolyte solution (pH 6.86 buffer); and (C) second scan (black) and 100th scan (red) from −0.1 to 0.8 V in a 0.1 M HCl solution. All CVs were recorded at a scan rate of 50 mV s⁻¹.

layer, since the peak intensity after desorption process still increases linearly with the layer number.

Figure 6 presents the plot of the peak intensities of amide I and symmetric OSO bands against the layer number for the multilayers fabricated from pH 6.0 SPANI and pH 9.8 G4NH₂ solutions. Desorption phenomenon was detected even during the deposition of this film. On comparison with the multilayer growth using pH 6.0 G4NH₂ solution, some differences were observed. There is a clear exponential increase in the peak intensities for the first few bilayers before a linear deposition region is reached, which should be related to the lower charge density of the G4NH₂ in pH 9.8 solution, and it takes about five bilayers to attain a steady-state charge reversal of the surface charge for a regular stepwise growth of the multilayers.[31,32] Furthermore, the amount of SPANI and G4NH₂ adsorption in these multilayers is larger than that of the films deposited from pH 6.0 G4NH₂ solution, which is due to the lower surface charge density of G4NH₂ at pH 9.8: Many dendrimers are needed to neutralize the surface charge of SPANI outmost layer.[18,58]

3.4. X-ray Reflectograms and Models of Molecular Arrangements in SPANI/G4NH₂ Multilayers. Figure 7 shows X-ray reflectograms (A) and electron density profiles (B) for four-bilayer films deposited from pH 6.0 and 9.8 G4NH₂ solutions, respectively. The data for the film prepared at pH 9.8 was offset by 1 decade for the sake of clarity. It can be observed that well-defined Kiessig fringes were detected for these two samples. The solid lines denote the best-fit calculated reflectivity to the experimental data. The thickness and

the error function respectively were estimated to be 6.9 and 0.72 nm for the film deposited from pH 6.0 G4NH₂ solution and 8.2 and 0.73 nm for the film from pH 9.8 G4NH₂ solution. The low error function proves that SPANI/G4NH₂ multilayers are uniform and flat. The average thickness per bilayer is 1.73 (pH 6.0) and 2.05 nm (pH 9.8) by dividing by the total number of bilayers. Both values are smaller than the diameter for an ideal spherical model of G4NH₂ with an extended conformation of all branches as estimated from molecular models[2,59] and also smaller than the diameter of G4NH₂ determined in solution,[8] which allows conclusion to be made about the highly compressed and flattened state of dendrimers within multilayers along the surface normal. This result is similar to the dendrimer monolayer and multilayer reported previously, in which the dendrimer has been highly compressed with an oblate shape determined by X-ray reflectivity, small-angle X-ray scattering, and AFM.[8,17,54,60] Another proposed explanation for the thinner thickness per bilayer is that the SPANI and G4NH₂ are highly interpenetrated between the layers, as opposed to forming discrete layers.

Since given the electron density profiles derived from the reflectivity data can provide more complete view of the internal structure of the multilayers,[61] the electron density profiles are presented in Figure 7B. For the film deposited from pH 9.8 G4NH₂ solution, oscillations can be detected over the whole film thickness. However, the oscillations for the film from pH 6.0 G4NH₂ solution damped progressively as the distance increases from the substrate, and the amplitude is also much larger than

the former, which indicates that the film prepared from pH 9.8 G4NH$_2$ solution has more ordered internal structure than the one deposited from pH 6.0 G4NH$_2$ solution. Considering the fact that the electron densities of SPANI and G4NH$_2$ are close to each other, the higher electron density of the film prepared from pH 6.0 G4NH$_2$ solution must indicate more dense packing within multilayer due to the high interpenetration. This idea is supported by the pH-dependent conformation changes of G4NH$_2$ as discussed below. At lower pH (6.0), the degree of ionization of G4NH$_2$ reaches close to 100%, and G4NH$_2$ takes an open structure with extended conformation of all branches.[53] The SPANI chain penetrates more easily into the interior part of the dendrimers, and the strong interpenetration between SPANI and G4NH$_2$ layers is expected (Figure 8A). However, at higher pH (9.8), only part of the terminals are charged and G4NH$_2$ has a condensed structure,[53] which makes the layer interpenetration lower, resulting in a more ordered multilayer (Figure 8B).

The surface roughness of the four-bilayer SPANI/G4NH$_2$ multilayers was also examined by AFM. In Figure 9, two images of the films prepared from pH 6.0 and 9.8 G4NH$_2$ solutions were recorded in tapping mode. Both samples were prepared with the same conditions with X-ray measurements. The root-mean-square value of the surface roughness as extracted from the commercial software was 0.72 nm (pH 6.0) and 0.39 nm (pH 9.8) nm within the 1 μm × 1 μm measurement region, respectively. Higher values of X-ray roughness are caused by the usual scale-dependent scaling behavior of real surfaces and the presence of macroscopic waves and defects that are not included in local areas selected on AFM images for roughness calculations.[8]

3.5. Redox Properties of SPANI/G4NH$_2$ Multilayers. Cyclic voltammograms (CVs) of the nine-bilayer multilayer in 0.1 M HCl along with the plots of $E_{1/2}$ against pH are shown in Figure 10. To obtain reproducible CVs, before potential scanning, the film was kept in an electrolyte solution for a period of time to allow complete permeation of the electrolyte into the polymer film. It can be seen that two couples of well-defined peaks corresponding to the redox processes at $E_{1/2}$ = 0.24 and 0.64 V were detected (Figure 10A) as in the voltammogram of the parent polyaniline,[61] while the peak shape is dramatically different from the parent polyaniline[61] and partly sulfonated polyaniline films.[46–50] In this multilayer, the first redox process ($E_{1/2}$ = 0.24 V) gives a couple of quite broad peaks, and the second one ($E_{1/2}$ = 0.64 V) results in a very sharp electrochemical response. It is worth noting here that on the first scan two anodic peaks (E_{OX2} = 0.65 and 0.69 V) were detected in the second redox region, which may be related to the different counterions combined with the cation radicals in the SPANI main chains. From the second scan the anodic peak at 0.69 V disappeared, and it should be a result of the self-doped SPANI. Hereafter, we discuss the redox properties using the steady-state redox peaks from the external acid (HCl) doping.

Analogous to those observed in the partly sulfonated polyaniline,[47,48,50] the $E_{1/2}$ values of both redox couples for SPANI are dependent on the pH in the acidic solutions (pH ≤ 2.0). The $E_{1/2}$ of the first redox peak shows a good linear relationship against pH with a slope of 42 mV/pH unit, whereas the second one shifts at the rate of −110 mV/pH as pH is smaller than 2.0 (Figure 10B). It has been reported that anions are inserted into

Scheme 2
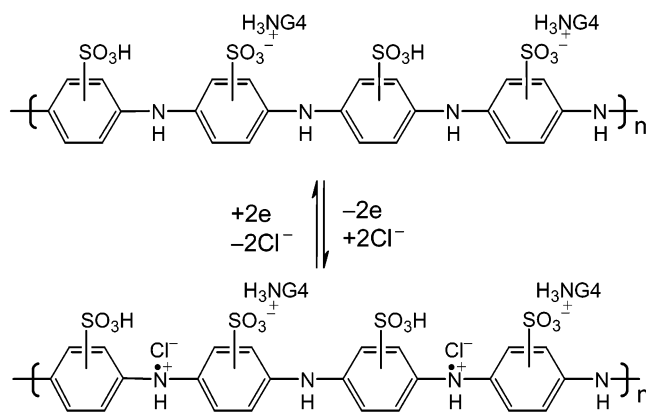
Scheme 3
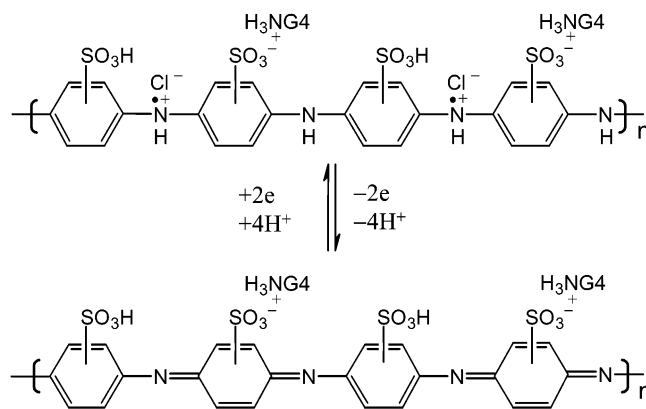
polyaniline films during oxidation,[62] and the results here verify this finding. Huang et al.[63] have proposed a model for polyaniline in which both oxidized and reduced forms can exist in protonated and deprotonated states. In Scheme 2, the reduced form is shown in its deprotonated state and the oxidized form in its protonated state. To simplify the discussion, we assume that a pH exists at which two forms of polyaniline are in these protonation states (Scheme 2). In this case, no protons are gained or lost in the multilayer during redox process. The creation of cationic sites (cation radicals) upon oxidation leads to a requirement of anion-compensating charges, which presumably come from the external supporting electrolyte. In this ideal state, one anion should be inserted for balancing the cationic site as one electron is removed. However, it has been shown that even at pH 1.0 the polyaniline is still partially protonated in its reduced form,[62] and the protonated sites will be neutralized by anions. On oxidation these sites will be deprotonated, so that the polymer can reach the resonance-stabilized structure (polaron structure) as shown in Scheme 2. To equilibrate the pH with solution, one expects that the protons migrate out of the film, leaving behind the anions that can serve to neutralize the protonated sites of the oxidized form. The remainder of the protonated sites will be compensated by insertion of additional anions. Therefore, the obvious deviation of 42 mV with respect to the 59 mV expected from theory according to Nernst equation may be attributed to the presence of partially protonated form in the reduced state. For the second redox couple at pH less than 2.0, the $E_{1/2}$ value changes at the rate of −110 mV/pH, which is almost consistent with the theoretical value (−118 mV), indicating that there are loss of two protons as one electron is removed (Scheme 3). The
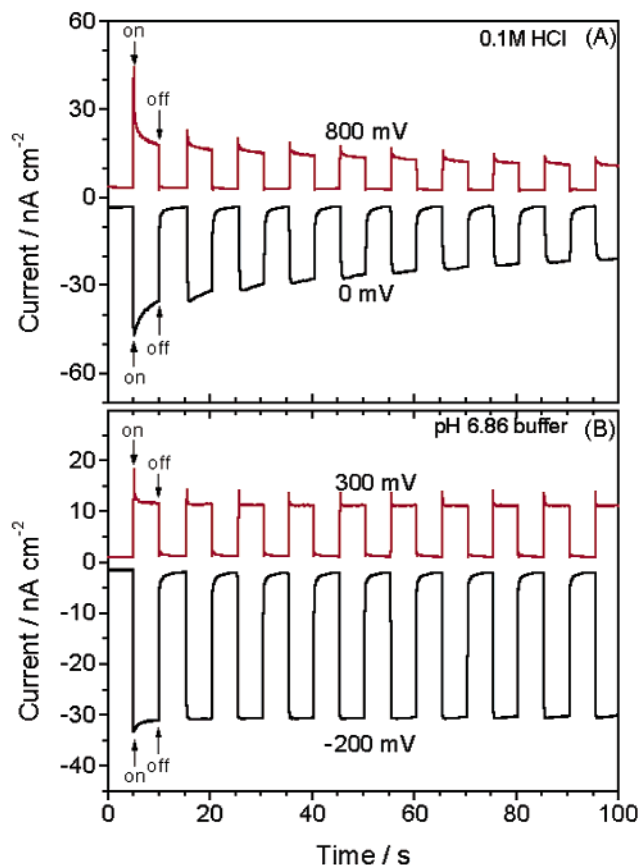
Figure 12. Photocurrent response of five-bilayer SPANI/G4NH$_2$ multilayers irradiated with polychromatic light. (A) In an aqueous 0.1 M HCl solution: red curve, 800 mV of bias; black curve, 0 mV. (B) In a pH 6.86 buffer (neutral) solution: red curve, 300 mV of bias; black curve, −200 mV.

discrepancies at higher pH values may be caused by the kinetic effect due to the lower proton concentration.

The stability of potential cycling of the nine-bilayer multilayers was measured in the acidic and neutral electrolytes (Figure 11). After 500 consecutive potential scans, the anodic current in 0.1 M HCl decreases by about 4% in the range of −0.1 to 0.4 V at 50 mV s^{-1} (Figure 11A), whereas in a neutral electrolyte solution (pH 6.86 buffer), 92% electroactivity was kept after cycling 500 scans in the range 0−0.3 V (Figure 11B). These results indicate that the SPANI/G4NH$_2$ multilayers have good physical and electrochemical stability in the acidic and neutral electrolyte solutions. However, when the potential is scanned to 0.8 V in 0.1 M HCl, irreversible degradation was detected, and a third redox couple ($E_{1/2}$ = 0.50 V) appeared between two original ones (Figure 11C) due to the hydrolysis of the imine to form benzoquinone, which is similar to the parent polyaniline.[62]

3.6. Photoelectric Conversion Properties of SPANI/G4NH$_2$ Multilayers. It is well-known that at the interface between semiconductor and an electrolyte solution photoelectrochemical effects can be observed.[64] In the present work, this effect was examined for SPANI/G4NH$_2$ multilayers under irradiation with polychromatic light. Figure 12 shows photocurrent response of five-bilayer multilayers coated on ITO electrode in acidic (A) and neutral (B) electrolyte solutions. Both anodic and cathodic photocurrents were detected, depending on the applied potentials. The observation of anodic photocurrent indicates that electrons flow from
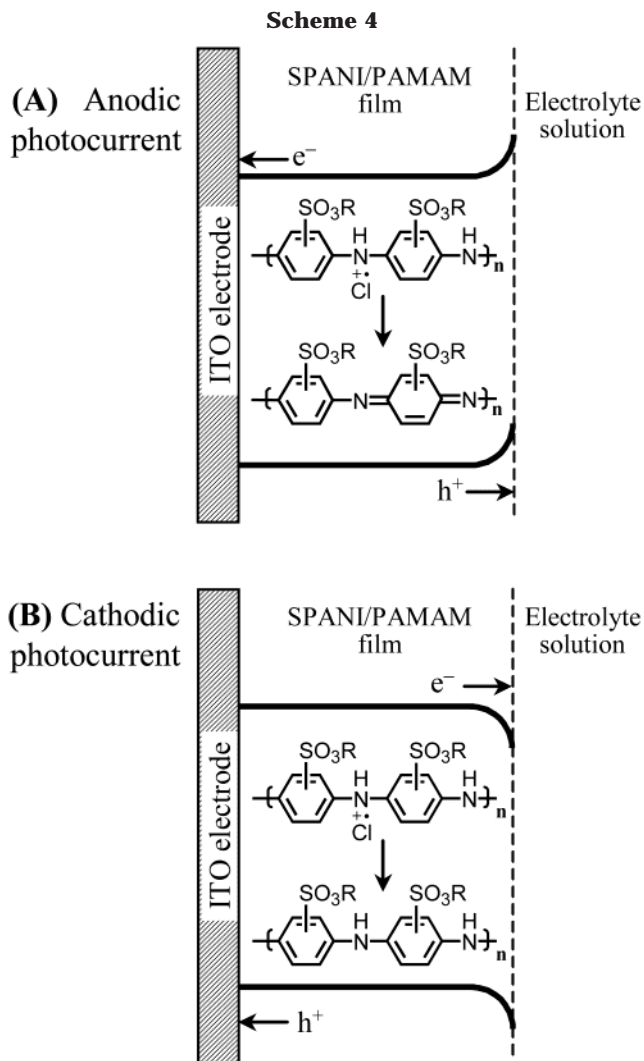
multilayers to electrode (as n-type semiconductor), whereas the cathodic photocurrent (as p-type semiconductor) is due to the electron flow from the electrode through the multilayer to the electrolyte solution (Scheme 4).[41,64,65] To further prove the electron-transfer process between the electrode and the multilayers, the effect of bias on the photocurrent was investigated. It shows that the anodic and cathodic photocurrents increase with the increase of the positive or negative bias (not shown here), indicating that the electron is transferred through the multilayer from an electrolyte solution to electrode or from electrode to the electrolyte solution, and the bias added on the electrode can promote electron transfer through these routines. These results can be readily attributed to the acceleration in the rate of charge separation,[41,65] resulting in an increasing proportion of the electron−hole pair separation occurring within the SPANI/G4NH$_2$ multilayers.

4. Conclusions

The conductive SPANI/G4NH$_2$ multilayers were successfully deposited onto solid substrates by electrostatic layer-by-layer assembly. The structure and properties of the multilayers were investigated by various physiochemical methods. It was found that the G4NH$_2$ dendrimers in the multilayers take a highly compressed conformation along surface normal. The thickness and molecular organization of the multilayers can be easily

controlled by adjusting the ion strength and pH of the dipping solutions. The highly physical and electrochemical stability in both acidic and neutral electrolyte solutions enables the potential applications of SPANI/G4NH$_2$ multilayers in biosensor and as electrocatalytic materials, since the G4NH$_2$ dendrimer has good biocompatibility and also can be used as host to encapsulate metal nanoparticles.

References and Notes

(1) Tomalia, D. A.; Baker, H.; Dewald, J.; Hall, M.; Kallos, G.; Martin, S.; Roeck, J.; Ryder, J.; Smith, P. *Polym. J.* **1985**, *17*, 117.

(2) Tomalia, D. A.; Naylor, A. M. Goddard, W. A. *Angew. Chem., Int. Ed. Engl.* **1990**, *29*, 138.

(3) Tomalia, D. A.; Durst, H. D. *Top. Curr. Chem.* **1993**, *165*, 193.

(4) Frechét, J. M. J. *Science* **1994**, *263*, 1710.

(5) Matthews, O. A.; Shipway, A. N.; Stoddart, J. F. *Prog. Polym. Sci.* **1998**, *23*, 1.

(6) Vögtle, F.; Gestermann, S.; Hesse, R.; Schwierz, H.; Windisch, B. *Prog. Polym. Sci.* **2000**, *25*, 987.

(7) Crooks, R. M.; Zhao, M.; Sun, L.; Chechik, V.; Yeung, L. K. *Acc. Chem. Soc.* **2001**, *34*, 181.

(8) Tsukruk, V. V.; Rinderspacher, F.; Bliznyuk, V. N. *Langmuir* **1997**, *13*, 2171.

(9) Zhao, M.; Tokuhisa, H.; Crooks, R. M. *Angew. Chem., Int. Ed. Engl.* **1997**, *36*, 2595.

(10) Tsukruk, V. V. *Adv. Mater.* **1998**, *10*, 253.

(11) He, J.-A.; Valluzzi, R.; Yang, K.; Dolukhanyan, T.; Sung, C.; Kumar, J.; Tripathy, S. K.; Samuelson, L.; Balogh, L.; Tomalia, D. A. *Chem. Mater.* **1999**, *11*, 3268.

(12) Wang, J.; Chen, J.; Jia, X.; Cao, W.; Li, M. *Chem. Commun.* **2000**, 511.

(13) Street, S. C.; Rar, A.; Zhou, J. N.; Liu, W. J.; Barnard, J. A. *Chem. Mater.* **2001**, *13*, 3669.

(14) Nagaoka, H.; Imae, T. *Int. J. Nonlinear Sci.* **2002**, *3*, 223.

(15) Wang, J.; Jia, X.; Zhong, H.; Luo, Y.; Zhao, X.; Cao, W.; Li, M.; Wei, Y. *Chem. Mater.* **2002**, *14*, 2854.

(16) Khopade, A. J.; Caruso, F. *Langmuir* **2002**, *18*, 7669.

(17) Ito, M.; Imae, T.; Aoi, K.; Tsutsumiuchi, K.; Noda, H.; Okada, M. *Langmuir* **2002**, *18*, 9757.

(18) Kim, B. Y.; Bruening, M. L. *Langmuir* **2003**, *19*, 94.

(19) Burroughes, J. H.; Bradley, D. D. C.; Brown, A. R.; Marks, R. N.; Mackay, K.; Friend, R. H.; Burns, P. L.; Holmes, A. B. *Nature (London)* **1990**, *347*, 539.

(20) McQuade, D. T.; Pullen, A. E.; Swager, T. M. *Chem. Rev.* **2000**, *100*, 2537.

(21) Raitman, O. A.; Katz, E.; Bückmann, A. F.; Willner, I. *J. Am. Chem. Soc.* **2002**, *124*, 6487.

(22) Shirakawa, H. *Angew. Chem., Int. Ed.* **2001**, *40*, 2575.

(23) MacDiarmid, A. G. *Angew. Chem., Int. Ed.* **2001**, *40*, 2581.

(24) Heeger, A. J. *Angew. Chem., Int. Ed.* **2001**, *40*, 2591.

(25) Shi, G.; Li, C.; Liang, Y. *Adv. Mater.* **1999**, *11*, 1145.

(26) Sadki, S.; Schottland, P.; Brodie, N.; Sabouraud, G. *Chem. Soc. Rev.* **2000**, *29*, 283.

(27) Nguyen, T. Q.; Martini, I. B.; Liu, J.; Schwartz, B. J. *J. Phys. Chem. B* **2000**, *104*, 237.

(28) Shi, Y.; Liu, J.; Yang, Y. *J. Appl. Phys.* **2000**, *87*, 4254.

(29) Wu, Z.; Wu, S.; Liang, Y. *Langmuir* **2001**, *17*, 7267.

(30) Kim, J.; Levitsky, I. A.; McQuade, D. T.; Swager, T. M. *J. Am. Chem. Soc.* **2002**, *124*, 7710.

(31) Decher, G. *Science* **1997**, *277*, 1232.

(32) Bertrand, P.; Jonas, A.; Laschewsky, A.; Legras, R. *Macromol. Rapid Commun.* **2000**, *21*, 319.

(33) Ferreira, M.; Rubner, M. F. *Macromolecules* **1995**, *28*, 7107.

(34) Fou, A. C.; Rubner, M. F. *Macromolecules* **1995**, *28*, 7115.

(35) Cheung, J. H.; Stockton, W. B.; Rubner, M. F. *Macromolecules* **1997**, *30*, 2712.

(36) Stockton, W. B.; Rubner, M. F. *Macromolecules* **1997**, *30*, 2717.

(37) Zotti, G.; Zecchin, S.; Berlin, A.; Schiavon, G.; Giro, G. *Chem. Mater.* **2001**, *13*, 43.

(38) DeLongchamp, D.; Hammond, P. T. *Adv. Mater.* **2001**, *13*, 1455.

(39) Lukkari, J.; Salomäki, M.; Viinikanoja, A.; Ääritalo, T.; Paukkunen, J.; Kocharova, N.; Kankare, J. *J. Am. Chem. Soc.* **2001**, *123*, 6083.

(40) Cutler, C. A.; Bouguettaya, M. Reynolds, J. R. *Adv. Mater.* **2002**, *14*, 684.

(41) Cao, T.; Wei, L.; Yang, S.; Zhang, M.; Huang, C.; Cao, W. *Langmuir* **2002**, *18*, 750.

(42) Baba, A.; Park, M.-K.; Advincula, R. C.; Knoll, W. *Langmuir* **2002**, *18*, 4648.

(43) Constantine, C. A.; Mello, S. V.; Dupont, A.; Cao, X.; Santos, D., Jr.; Oliveira, O. N., Jr.; Strixino, F. T.; Pereira, E. C.; Cheng, T.-C.; Defrank, J. J.; Leblanc, R. M. *J. Am. Chem. Soc.* **2003**, *125*, 1805.

(44) Sebastian, R.-M.; Caminade, A. M.; Majoral, J.-P.; Levillain, E.; Huchet, L.; Roncali, J. *Chem. Commun.* **2000**, 507.

(45) Alvarez, J.; Sun, L.; Crooks, R. M. *Chem. Mater.* **2002**, *14*, 3995.

(46) Yue, J.; Epstein, A. J. *J. Am. Chem. Soc.* **1990**, *112*, 2880.

(47) Yue, J.; Wang, Z. H.; Cromack, K. R.; Epstein, A. J.; MacDiarmid, A. G. *J. Am. Chem. Soc.* **1991**, *113*, 2665.

(48) Wei, X.-L.; Wang, Y. Z.; Long, S. M.; Bobeczko, C.; Epstein, A. J. *J. Am. Chem. Soc.* **1996**, *118*, 2545.

(49) Chen, S.-A.; Hwang, G.-W. *Macromolecules* **1996**, *29*, 3950.

(50) Takahashi, K.; Nakamura, K.; Yamaguchi, T.; Komura, T.; Ito, S.; Aizawa, R.; Murata, K. *Synth. Met.* **2002**, *128*, 27.

(51) McCall, R. P.; Ginder, J. M.; Leng, J. M.; Ye, H. J.; Manohar, S. K.; Masters, J. G.; Asturias, G. E.; MacDiarmid, A. G.; Epstein, A. J. *Phys. Rev. B* **1990**, *41*, 5202.

(52) Welch, P.; Muthukumar, M. *Macromolecules* **1998**, *31*, 5892.

(53) Chen, W.; Tomalia, D. A.; Thomas, J. L. *Macromolecules* **2000**, *33*, 9169.

(54) Betley, T. A.; Holl, M. M. B.; Orr, B. G.; Swanson, D. R.; Tomalia, D. A.; Baker, J. R. *Langmuir* **2001**, *17*, 2768.

(55) Manna, A.; Imae, T.; Aoi, K.; Okada, M.; Yogo, T. *Chem. Mater.* **2001**, *13*, 1674.

(56) Furukawa, Y.; Ueda, F.; Hyodo, Y.; Harada, I.; Nakajima, T.; Kawagoe, T. *Macromolecules* **1988**, *21*, 1297.

(57) Ariga, K.; Lvov, Y.; Kunitake, T. *J. Am. Chem. Soc.* **1997**, *119*, 2224.

(58) Shiratori, S. S.; Rubner, M. F. *Macromolecules* **2000**, *33*, 4213.

(59) Li, J.; Piehler, L. T.; Qin, D.; Baker, J. R.; Tomalia, D. A. *Langmuir* **2000**, *16*, 5613.

(60) Li, X.; Imae, T.; Leisner, D.; López-Quintela, M. A. *J. Phys. Chem. B* **2002**, *106*, 12170.

(61) Arys, X.; Fischer, P.; Jonas, A. M.; Koetse, M. M.; Laschewsky, A.; Legras, R.; Wischerhoff, E. *J. Am. Chem. Soc.* **2003**, *125*, 1859.

(62) Orata, D.; Buttry, D. A. *J. Am. Chem. Soc.* **1987**, *109*, 3574.

(63) Huang, W.-S.; Humphrey, B. D.; MacDiarmid, A. G. *J. Chem. Soc., Faraday Trans. 1* **1986**, *82*, 2385.

(64) Maia, D. J.; das Neves, S.; Alves, O. L.; De Paoli, M.-A. *Electrochim. Acta* **1999**, *44*, 1945.

(65) Cao, T.; Yang, S.; Cao, J.; Zhang, M.; Huang, C.; Cao, W. *J. Phys. Chem. B* **2001**, *105*, 11941.